JBC RESEARCH ARTICLE

# Rab8 and TNPO1 are ciliary transport adaptors for GTPase Arl13b by interacting with its RVEP motif containing ciliary targeting sequence

Received for publication, August 24, 2022, and in revised form, March 4, 2023 Published, Papers in Press, March 11, 2023,
https://doi.org/10.1016/j.jbc.2023.104604

**Divyanshu Mahajan**[‡], **Viswanadh Madugula**[‡], **and Lei Lu**[*]
*From the School of Biological Sciences, Nanyang Technological University, Singapore*

Reviewed by members of the JBC Editorial Board. Edited by Phyllis Hanson

**Arl13b, an ARF/Arl-family GTPase, is highly enriched in the cilium. Recent studies have established Arl13b as one of the most crucial regulators for ciliary organization, trafficking, and signaling. The ciliary localization of Arl13b is known to require the RVEP motif. However, its cognate ciliary transport adaptor has been elusive. Here, by imaging the ciliary localization of truncation and point mutations, we defined the ciliary targeting sequence (CTS) of Arl13b as a C-terminal stretch of 17 amino acids containing the RVEP motif. We found Rab8-GDP, but not Rab8-GTP, and TNPO1 simultaneously and directly bind to the CTS of Arl13b in pull-down assays using cell lysates or purified recombinant proteins. Furthermore, Rab8-GDP substantially enhances the interaction between TNPO1 and CTS. Additionally, we determined that the RVEP motif is an essential element as its mutation abolishes the interaction of the CTS with Rab8-GDP and TNPO1 in pull-down and TurboID-based proximity ligation assays. Finally, the knockdown of endogenous Rab8 or TNPO1 decreases the ciliary localization of endogenous Arl13b. Therefore, our results suggest Rab8 and TNPO1 might function together as a ciliary transport adaptor for Arl13b by interacting with its RVEP-containing CTS.**

The primary cilium (hereafter referred to as cilium) is a specialized microtubule-based plasma membrane (PM) protrusion. It functions as a cell's antenna to sense environmental stimuli and initiate diverse intracellular responses (1, 2). The sensory function of the cilium critically depends on the ciliary localization of receptors and their signaling accessories. Genetic disorders compromising such localization can cause diverse human diseases collectively called ciliopathies (3–5). How ciliary proteins are specifically targeted to the cilium is one of the most fundamental questions in cilium biology.

The ciliary targeting of many proteins requires the ciliary targeting sequence (CTS), a short array of amino acids recognized by the ciliary transport adaptor (4, 6–9). However, unlike membrane trafficking sorting signals, there seem to be no significant consensus sequences among known CTSs. Compared to cargo adaptors involved in membrane trafficking, we know much less about the ciliary transport adaptors—what they are and how they transport CTS-containing cargos. One of the most studied ciliary transport adaptors is Tulp3. It has been proposed as the adaptor for multiple ciliary membrane proteins, including various GPCRs, polycystin 1/2 complex, and fibrocystin (10–15).

Importins, such as importin-β1 and transportin1 (TNPO1), were uncovered as Ran GTPase-regulated adaptors for the ciliary targeting of Crumbs3, Kif17, and retinitis pigmentosa 2 (RP2) (16, 17). On the other hand, Rab8-GDP was demonstrated to target fibrocystin to the cilium by binding to its CTS (18). Based on these results, we further found that Rab8-GDP and TNPO1 could function together as a ciliary transport adaptor for fibrocystin, photoreceptor retinol dehydrogenase (prRDH), rhodopsin, and RP2 (19). Rab8-GDP, but not Rab8-GTP, and TNPO1 simultaneously interact with CTSs of these ciliary membrane proteins to form a ternary complex. Our model proposes that the ternary complex first transports the cargo across the membrane diffusion barrier at the cilium base. Once inside the cilium, Rab8 undergoes the guanine nucleotide exchange from the GDP to GTP form by the guanine nucleotide exchange factor of Rab8. As a result, the ternary complex disassembles, releasing the free cargo at the ciliary membrane (6, 19).

Arl13b is an ARF/Arl family small GTPase highly enriched in the cilium (20). Mutation in the *ARL13B* gene can lead to Joubert syndrome, a genetic disorder characterized by kidney cysts, retinal degeneration, skeletal change, and brain malfunctions (21). Studies suggest that Arl13b has multiple roles in ciliary assembly, organization, trafficking, and sensory functions. For example, depletion or knockout of Arl13b results in reduced ciliogenesis, shortened cilium length, and impaired sonic hedgehog signaling (20, 22, 23). Furthermore, Arl13b can recruit the lipid phosphatase INPP5E to the cilium (24). At the ciliary membrane, INPP5E converts PI(4,5)$P_2$ to PI4P (25, 26), an essential process for the release of cargo from Tulp3 (10). Consequently, INPP5E is required for ciliary trafficking and Hedgehog signaling (25, 26). Arl13b can also function as a guanine nucleotide exchange factor to activate Arl3, another ARF/Arl family small GTPase (27). The active or GTP-loaded Arl3 can subsequently facilitate the ciliary

[‡] These authors contributed equally to this work.
[*] For correspondence: Lei Lu, lulei@ntu.edu.sg.

transport of lipidated proteins by releasing them from transporters such as PDE6δ and Unc119a/b (28–30).

The ciliary localization of Arl13b is critical for its cellular functions, but the molecular and cellular mechanism behind its ciliary targeting remains obscure. Tulp3 is required for the proper ciliary localization of Arl13b (31–33), possibly by interacting with Arl13b's N-terminal amphipathic helix (34). In addition, the C-terminal RVEP motif has been known to play an essential role in the ciliary localization of Arl13b (23, 35–38). However, the ciliary transport adaptor that recognizes the RVEP motif of Arl13b is still unknown. In this study, we defined the Arl13b CTS, which contains the previously uncovered RVEP motif. Furthermore, our data suggest that Rab8-GDP and TNPO1 simultaneously bind to the CTS in an RVEP motif-dependent manner to function as a ciliary transport adaptor for Arl13b.

## Results

### The CTS of Arl13b resides at its C-terminal half

Arl13b is an atypical ARF/Arl family GTPase (39–42). In addition to the GTPase domain, it has an N-terminal lipid-anchor region, a common feature shared among most ARF/Arl family members, and an unusually long C-terminus. Hence, the coding sequence of Arl13b comprises, from the N to C-terminus, the lipid-anchor region, the GTPase domain, a coiled-coil region (CC), an intrinsically disordered region (IDR), the RVEP motif, and a proline-rich region (PRR) (Fig. 1*A*). We found that mutating RVEP to AAAA (RVEP-4A) substantially reduced the ciliary localization of the full-length Arl13b in ciliated RPE1 cells (Fig. 1*A*), consistent with previous reports (23, 35–38). We quantified the ciliary localization of the WT and RVEP-4A mutant using the cilium to the PM intensity ratio (*CPIR*), an expression level-independent metric to quantitatively measure the ciliary localization (19). Figure 1*B* schematically illustrates calculating the *CPIR* of PM-localized transmembrane protein using an image showing the cilium, PM, and background (non-cell area). First, a line of ∼1 μm in width was drawn orthogonally across the cilium. Next, the maximum intensity of the line intensity profile ($I_{max}$), the mean intensity of the PM ($I_{PM}$), and the mean intensity of the background ($I_{background}$) were acquired. Then, the *CPIR* of the transmembrane protein is calculated as $CPIR = (I_{max} - I_{PM})/(I_{PM} - I_{background})$.

Surface labeling is usually employed to specifically highlight the PM and cilium pools of a PM-localized transmembrane protein (for example, CD8a-fusion chimeras, see below), but it requires that the ciliary protein of interest has a detectable extracellular domain. Since Arl13b and its mutants are peripheral membrane proteins without an extracellular domain, their PM intensities could also be contributed by their intracellular pools, such as the ER, endosomal, and cytosolic pools, which our imaging could not resolve. Therefore, the *CPIR* of Arl13b and its mutants reflects the relative cilium enrichment to the cellular but not the PM pool. By quantification, we observed that the *CPIR* of full-length Arl13b was reduced by almost 20-fold upon RVEP-4A mutation, in contrast to the WT (Fig. 1*C*), confirming that the RVEP motif is essential for the ciliary targeting of Arl13b.

The CTS should be defined as a short sequence that is both necessary and sufficient for ciliary targeting. Hence, from previous reports and our data, we reasoned that the CTS of Arl13b must localize to a C-terminal region containing the RVEP motif. To precisely map the CTS, we constructed a series of C-terminally GFP-tagged mutants of Arl13b with truncation or point mutation (Fig. 1*A*). Western blotting of cell lysates transiently transfected with these constructs confirmed the expression of these mutants (Fig. S1*A*). We found that except for Arl13b without the CC (ΔCC), Arl13b truncation mutants such as ΔGTPase (the majority of which comprises the C-terminal half), ΔIDR, and ΔPRR displayed robust ciliary localization (Fig. 1*A*). On the other hand, the N-terminal half fragment or amino acids (AAs) 1-245 (AA1-245-GFP), which contains the N-terminal lipid-anchor region, GTPase domain, and CC, had a very weak ciliary localization. Its *CPIR* decreased by almost 20-fold compared to the WT (Fig. 1, *A* and *C*). Therefore, the CTS of Arl13b must reside in the C-terminal half, comprising AAs 245-428.

### A C-terminal 17 amino acid fragment with the RVEP motif contains the CTS

However, we observed that the C-terminal half fragment, AA245-428, did not localize to the cilium (Fig. 1*A*). The negative ciliary localization of AA245-428 is possibly due to its lack of membrane anchorage since several previous studies demonstrated the essential role of the N-terminal palmitoylation (35, 43, 44). Using cysteine to serine mutation (C8S/C9S) to abolish all potential palmitoylation sites within the N-terminus of Arl13b (Figs. 1*A* and S1*A*), we confirmed the previous result (Fig. 1*A*). To anchor AA245-428 to the PM, we wanted to establish a small N-terminal palmitoylation region of Arl13b and graft it to the fragment AA245-428. When the N-terminal palmitoylation sequence from AAs one to 9 (hereafter referred to as PAL) (Figs. 1*A* and 2*A*) was fused to the N-terminus of the GFP, the resulting fusion protein, PAL-GFP, localized to the PM (Fig. 2*B*), Golgi, and lysosome (Fig. 2*C*) but not the cilium (Fig. 2*D*). When C8S/C9S mutations were introduced, PAL-C8S/C9S-GFP lost its PM, Golgi, and lysosome localization (Fig. 2, *B* and *C*). Therefore, PAL is sufficient for membrane anchorage of a reporter to the PM, possibly by palmitoylation.

We then fused PAL to the N-terminus of AA245-428 and investigated the resulting fusion protein's localization. Indeed, we observed a robust ciliary localization for PAL-AA245-428-GFP (Fig. 2*E*), supporting that AA245-428 should contain the CTS. We subsequently made further serial truncation of AA245-428 and similarly tagged the resulting fragments with PAL and GFP (Fig. 2*E*). When RPE1 cell lysates expressing these fragments were subjected to Western blotting, all

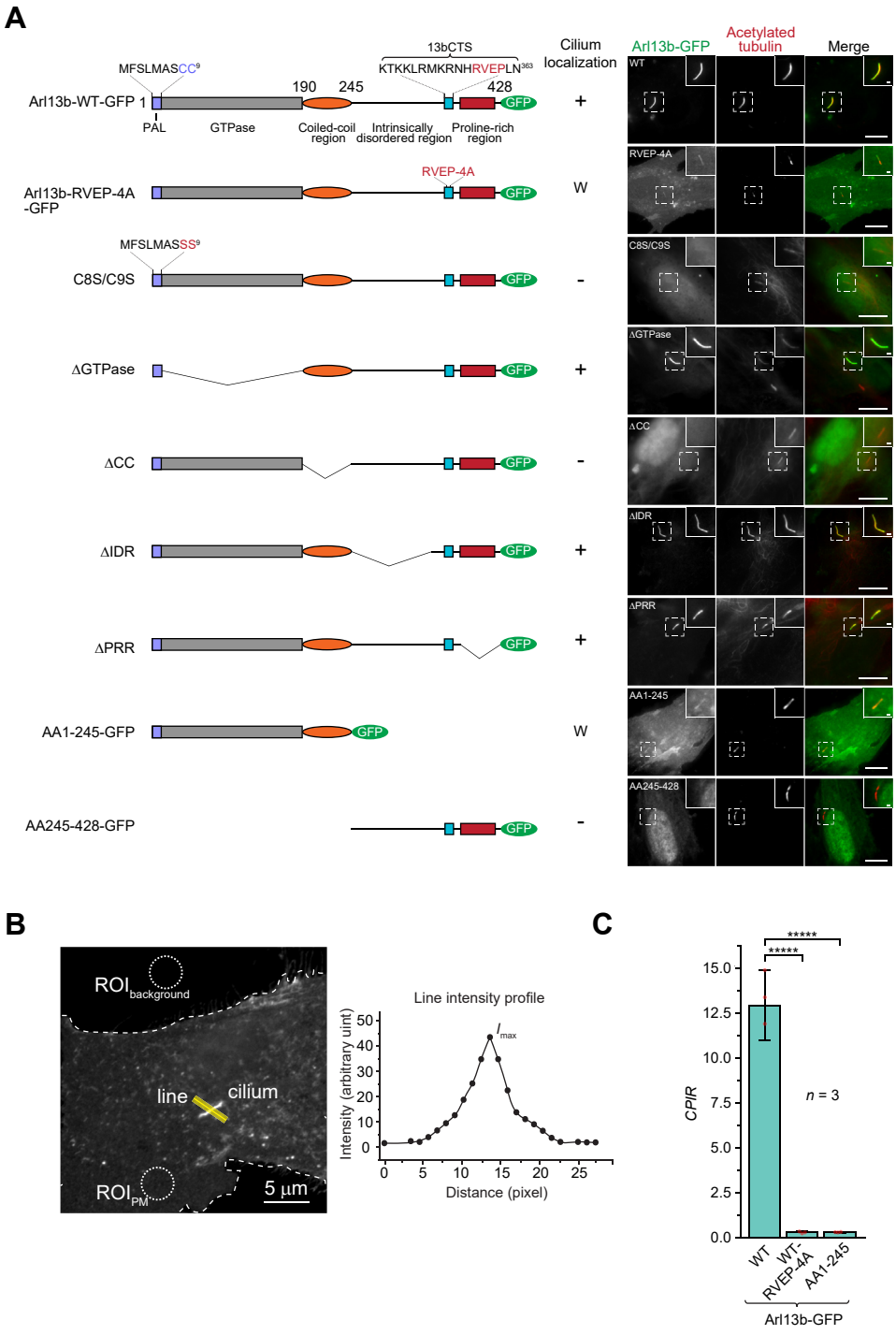


**Figure 1. The CTS of Arl13b resides at its C-terminal half.** All cells were RPE1 cells. *A*, domain organization and ciliary localization of Arl13b and its mutants. A schematic diagram illustrating the domain organization of Arl13b and its mutants is shown on the *left*. On the *right*, cells transiently expressing Arl13b and its mutants were immunostained for acetylated tubulin, a cilium marker. Scale bar, 10 μm. The cilium is enlarged and boxed at the *upper right corner* in these images. Scale bar, 1 μm. In the *middle* column, the ciliary localization was qualitatively scored based on the fluorescence imaging shown on the *right* as strongly positive (+), weakly positive (W), and negative (–). *B*, a diagram schematically demonstrating the calculation of the *CPIR* of a ciliary membrane protein. The image at the *left* shows part of a cell transiently expressing the ciliary transmembrane protein. *Dotted lines* mark the cell contour. $I_{PM}$ and $I_{background}$ are calculated from the $ROI_{PM}$ and $ROI_{background}$, which are marked by *dotted circles*. A *yellow line* with a width of ~ 1 μm is drawn across the cilium to measure the line intensity profile. The plot at the *right* shows the corresponding line intensity profile with the peak intensity, $I_{max}$. *C*, a bar graph showing the *CPIR* values of WT and selected mutants of Arl13b from (*A*). Data were from $n = 3$ independent experiments, with each experiment having >30 cilium and GFP-positive cells analyzed. The error bar represents the mean ± SD. *p*-values are from unpaired, two-tailed *t*-tests; *****$p \le 0.000005$. CPIR, cilium to the PM intensity ratio.

fragments, including AA245-428, migrated with the expected molecular weights (Fig. S1*B*), suggesting the correct expression of these fragments. Although PAL has been reported to be part of the CTS of Arl13b (34), the negative or weak ciliary localization of PAL-GFP, AA1-245-GFP, PAL-AA245-325-GFP, PAL-AA347-363-RVEP-4A-GFP, and Arl13b-RVEP-4A-GFP

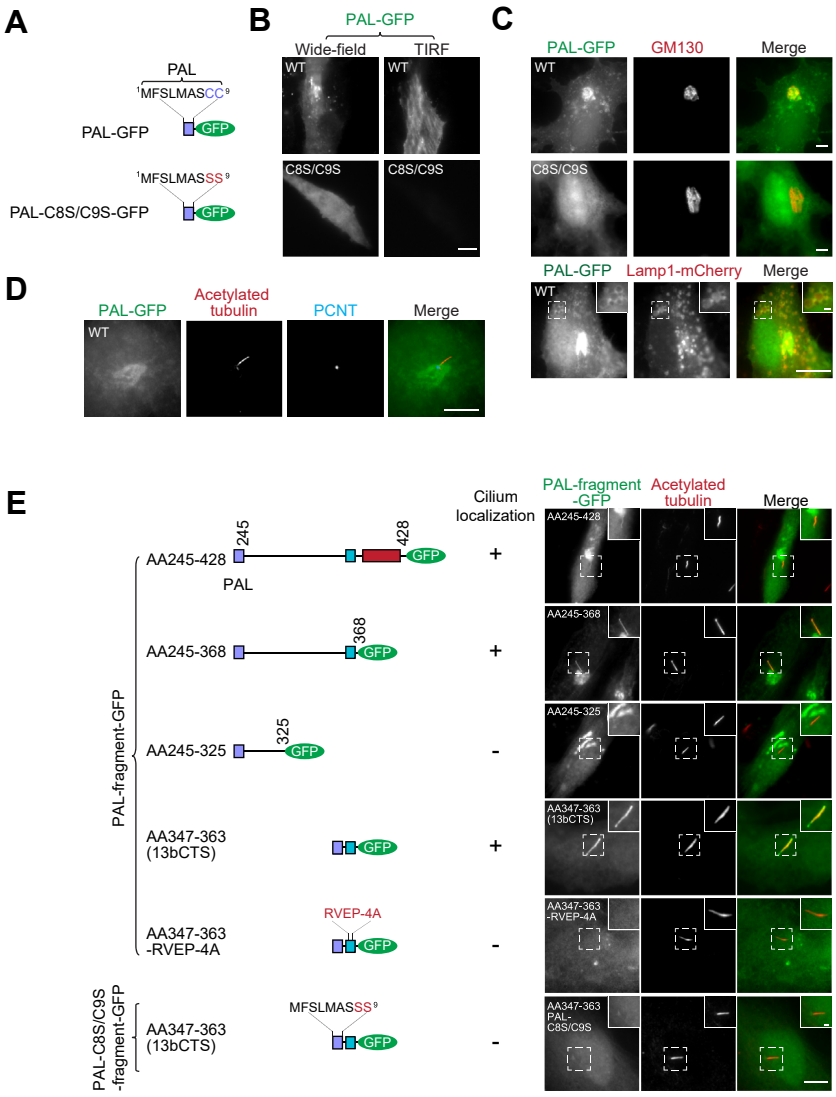


**Figure 2. A C-terminal 17 amino acid fragment with the RVEP motif contains the CTS.** All cells are RPE1 cells. *A*, domain organization of PAL-GFP and PAL-C8S/C9S-GFP. *B* and *C*, PAL is a potential membrane anchorage sequence that targets GFP to the PM, Golgi, and lysosome. In (*B*), the same live RPE1 cell transiently expressing PAL-GFP or PAL-C8S/C9S-GFP was first imaged under the wide-field mode, followed by the total internal reflection fluorescence (TIRF) mode. Only the PM is visible under the TIRF mode. In (*C*), RPE1 cells transiently expressing PAL-GFP or PAL-C8S/C9S-GFP were immunostained for endogenous GM130 (a Golgi marker) (*top and middle rows*). Alternatively, cells transiently co-expressing PAL-GFP and Lamp1-mCherry (a lysosome marker) were directly imaged after fixation (*bottom row*). The box region is enlarged in the *upper right corner* to show the localization of PAL-GFP to the lysosome. *D*, PAL does not target GFP to the cilium. RPE1 cells transiently expressing PAL-GFP were immunostained for endogenous acetylated tubulin and PCNT, a centrosome marker. *E*, domain organization and ciliary localization of PAL-fused truncation fragments of AA245-428. A schematic diagram illustrating the domain organization is shown on the *left*. These fragments are fused to the C-terminus of PAL and the N-terminus of GFP to make PAL-fragment-GFP. The ciliary localization was qualitatively scored based on the fluorescence imaging shown on the *right*, similar to Figure 1*A*. The box region is enlarged in the *upper right corner* to show the cilium. Scale bar, 10 μm. Scale bar for boxed region in (*C*) and (*E*), 1 μm.

(Figs. 1*A* and 2, *D* and *E*) indicated that PAL does not confer specific ciliary localization. Therefore, Arl13b C-terminal fragments should determine the ciliary localization. Furthermore, we found that the PAL and GFP-fused fragment (PAL-fragment-GFP) without the RVEP motif (Fig. 2*E*), AA245-325, did not localize to the cilium. On the other hand, those with the motif, including AA245-368 and AA347-363 but not AA347-363-RVEP-4A, displayed strong ciliary localization. Note that the bright lump near the ciliary base in AA245-428, AA245-368, and AA245-325 images (Fig. 2*E*) should be the Golgi similar to PAL-GFP (Fig. 2*C*). Therefore, AA347-363, a fragment comprising 17 AAs including the RVEP motif, must contain the CTS of Arl13b.

### *The C-terminal 17 amino acid fragment targets CD8a to the cilium*

CD8a is a type I transmembrane protein with a short C-terminal cytosolic tail. The C-terminally GFP-tagged CD8a displayed a non-specific and weak ciliary localization (19). To further characterize the ciliary targeting of AA347-363, we constructed a series of chimeras comprising sequentially from the N to C-terminus the following three parts—CD8a without the cytosolic tail, an AA347-363 fragment with truncation or point mutations, and the GFP tag (Fig. 3*A*). Western blot of cell lysates transiently transfected with these constructs confirmed these mutants' expression (Fig. S1*B*). We found that, compared to CD8a, the CD8a chimera with AA347-363

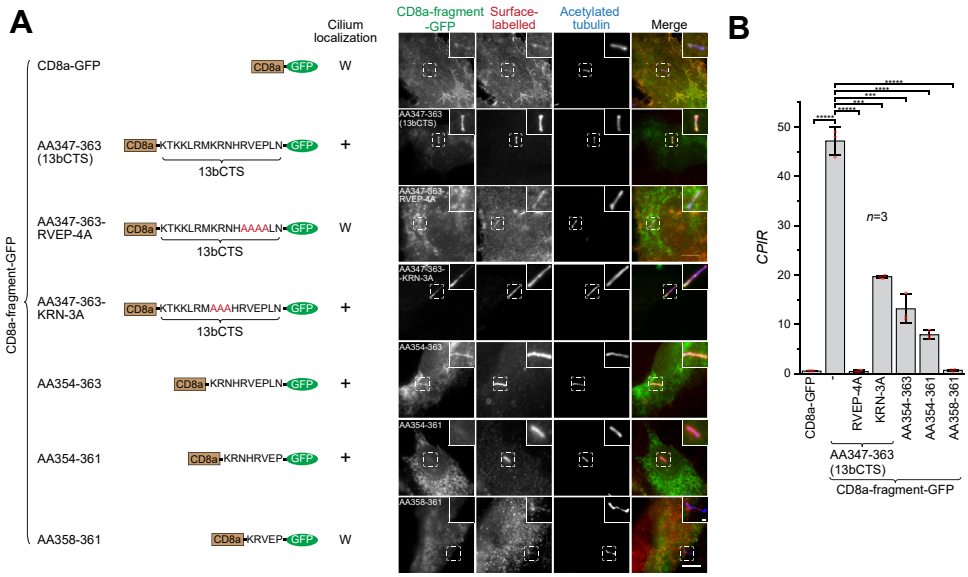


**Figure 3. The C-terminal 17 amino acid fragment with the RVEP motif targets CD8a to the cilium.** All cells are RPE1 cells. *A*, domain organization and ciliary localization of CD8a-fused truncation fragments of AA347-363. A schematic diagram illustrating the domain organization is shown on the *left*. These fragments are fused to the C-terminus of cytosolic tail-deleted CD8a and the N-terminus of GFP. The ciliary localization was qualitatively scored based on the fluorescence imaging shown on the *right*, similar to Figure 1*A*. In the *right* panel image, surface staining of CD8a (surfaced-labeled) was employed to reveal the ciliary localization of the chimeras. Scale bar, 10 μm. The cilium is enlarged and boxed at the *upper right corner* in these images. Scale bar, 1 μm. *B*, a bar graph showing the *CPIR* values of CD8a-chimeras. Data were from $n = 3$ independent experiments, with each experiment having >30 cilium and GFP-positive cells analyzed. The error bar represents the mean ± SD. *p*-values are from unpaired, two-tailed *t*-tests; ***$p \le 0.0005$; ****$p \le 0.00005$; *****$p \le 0.000005$.

but not AA347-363-RVEP-4A displayed an ∼80-fold increase in the *CPIR* (Fig. 3, *A* and *B*). Hence, our data indicate that AA347-363 is sufficient to target a transmembrane reporter to the cilium. Next, we truncated AA347-363 from N- and C-terminus to make CD8a and GFP-fused AA354-363, AA354-361, and AA358-361 (Fig. 3*A*). We found that decreasing the length of AA347-363 reduced *CPIR*s of the resulting fragments by more than threefold (Fig. 3*B*). Among our truncations chimeras, AA354-361 was the smallest fragment that had a significant ciliary localization (Fig. 3*B*). When the KRN motif of AA347-363 was mutated to AAA (KRN-3A), we observed the *CPIR* of the resulting chimera decreased by more than 2-fold, though it was still almost 40-fold higher than that of the RVEP-4A mutant. Since further truncation and mutagenesis of AA347-363 substantially reduce its *CPIR*, AA347-363 is essential for highly efficient and robust ciliary targeting. Together with its sufficiency in ciliary targeting, we define AA347-363 as the CTS of Arl13b, hereafter referred to as 13bCTS.

### *Rab8 and TNPO1 simultaneously and synergistically interact with Arl13b* via *13bCTS*

We next attempted to find the transport adaptor for 13bCTS. We previously discovered that Rab8 and TNPO1 interact with the CTSs of several ciliary membrane proteins and function as their ciliary transport adaptor (19). We investigated their interactions *via* pull-down assays to test if Rab8 and TNPO1 act as the ciliary transport adaptor for 13bCTS. First, we transfected HEK293T cells with C-terminally GFP-tagged Arl13b-WT, Arl13b-RVEP-4A, or RP2 (positive control) (19) (Fig. 4*A*). Next, the resulting cell lysates were individually incubated with bead-immobilized GST-Rab8-T22N or GST-Rab8-Q67L (Fig. S1*C*). Q67L and T22N (hereafter referred to as QL and TN respectively) are point mutations that lock Rab8 in the GTP and GDP-bound form respectively (45). Finally, we analyzed bead-retained proteins by immunoblotting. We found that GST-Rab8-TN specifically pulled down RP2 and Arl13b-WT but not Arl13b-RVEP-4A (Fig. 4*A*). Interestingly, bead-immobilized GST-Rab8-TN pulled down a substantial amount of endogenous TNPO1 under the expression of Arl13b-WT (Lane 4), but not Arl13b-RVEP-4A (Lane 6). Our data demonstrate that Rab8-GDP and TNPO1 could interact with Arl13b in cultured cells.

To test if the interaction is direct and determine the interacting region of Arl13b, we prepared N-terminally His-tagged recombinant proteins, His-AA1-245-GFP and His-AA193-428-GFP, corresponding to the N and C-terminal halves of Arl13b (Figs. 4*B* and S1*C*). When bead-immobilized GST-Rab8-TN or -QL was incubated with the two His-tagged proteins, we found that His-AA193-428, but not His-AA1-245, was specifically retained on GST-Rab8-TN beads, demonstrating that Rab8-TN alone directly interacted with His-AA193-428 (Fig. 4*C*). Similarly, when bead-immobilized GST-TNPO1 (Fig. S1*C*) was incubated with the two His-tagged proteins, we found that TNPO1 alone directly interacted with His-AA193-428 but not His-AA1-245 (Lane one and two of Fig. 4*D*). The interaction between GST-TNPO1 and His-AA193-428 was substantially enhanced in the presence of His-Rab8-TN but not His-Rab8-QL (Lane five and six of Fig. 4*D*), suggesting a synergistic effect between Rab8-TN and TNPO1 on the interaction with His-AA193-428.

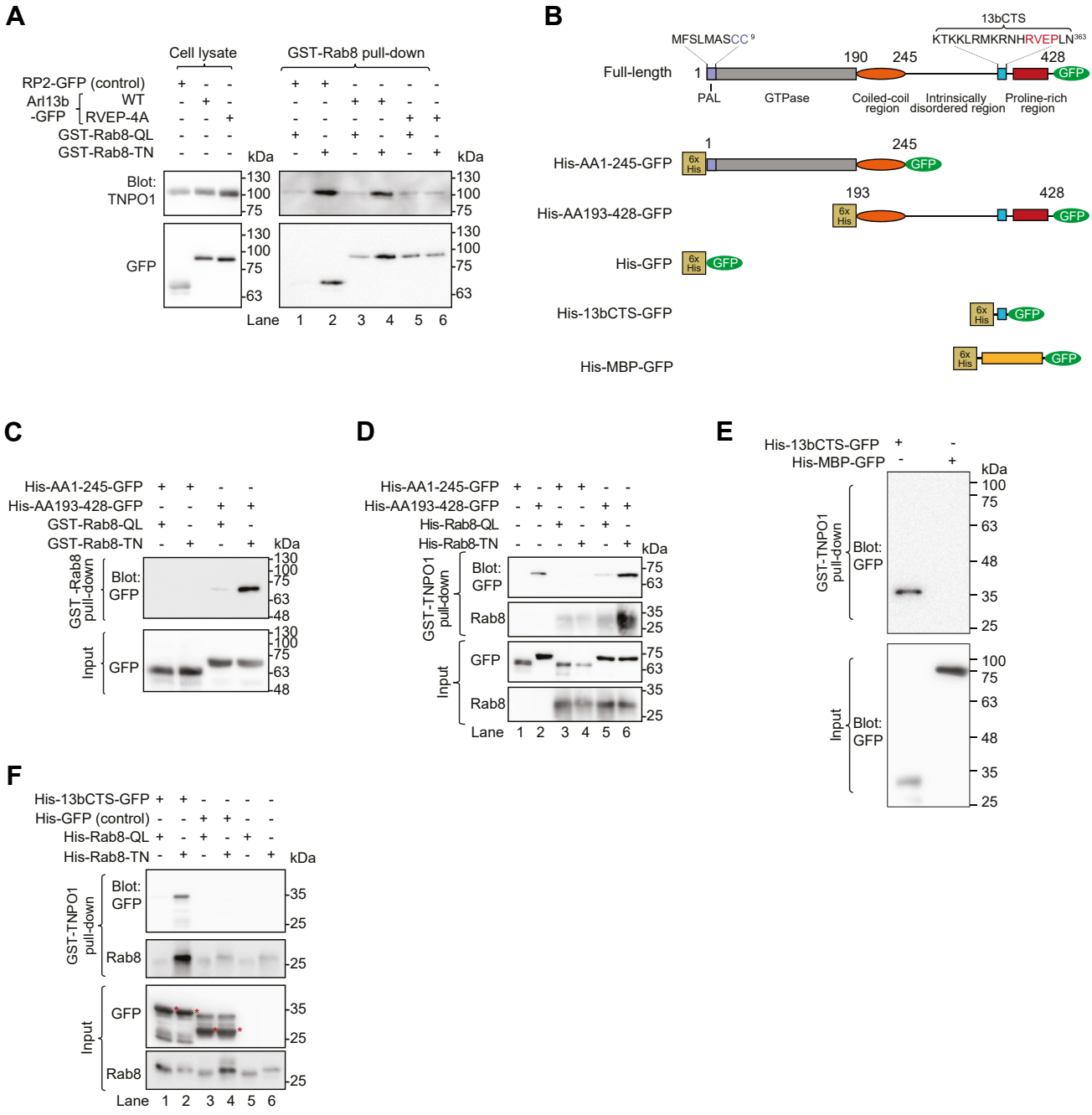


**Figure 4. Rab8, TNPO1, and 13bCTS form a ternary complex.** All cell lysates were from HEK293T cells. *A*, Rab8-TN interacts with Arl13b and TNPO1 in an RVEP motif-dependent manner. Bead-immobilized GST-Rab8-TN and GST-Rab8-QL were incubated with cell lysates transiently expressing RP2-GFP (positive control), Arl13b-WT-GFP, or Arl13b-RVEP-4A, and the proteins retained were analyzed by immunoblotting. *B*, a schematic diagram illustrating various recombinant His-tagged Arl13b fragments used in the below pull-down assays. *C*, Rab8-TN interacts with the C-terminal half of Arl13b. Bead-immobilized GST-Rab8-TN and GST-Rab8-QL were incubated with purified His-tagged N (His-AA1-245-GFP) or C-terminal half of Arl13b (His-AA193-428-GFP), followed by immunoblotting similar to (*A*). *D*, TNPO1 interacts with the C-terminal half of Arl13b in a Rab8-TN-dependent manner. Bead-immobilized GST-TNPO1 was incubated with purified His-tagged Rab8-TN, Rab8-QL, N (His-AA1-245-GFP), or C-terminal half of Arl13b (His-AA193-428-GFP), followed by immunoblotting similar to (*A*). *E*, TNPO1 interacts with 13bCTS. Bead-immobilized GST-TNPO1 was incubated with purified His-13bCTS-GFP or His-MBP-GFP (negative control), followed by immunoblotting similar to (*A*). *F*, TNPO1 interacts with 13bCTS in a Rab8-TN-dependent manner. Bead-immobilized GST-TNPO1 was incubated with purified His-tagged Rab8-TN, Rab8-QL, 13bCTS, or control, followed by immunoblotting similar to (*A*). * indicates the specific band. Molecular weight markers are labeled to the *right* of all immunoblots.

Furthermore, we also observed that GST-TNPO1 pulled down His-Rab8-TN only in the presence of His-AA193-428 but not His-AA1-245 (Lane four and six of Fig. 4*D*), suggesting that the interaction between TNPO1 and Rab8-TN might become significant *via* their simultaneous binding to AA193-428. In summary, our results support that Rab8-TN and TNPO1 can simultaneously and synergistically interact with Arl13b C-terminus.

We tested if 13bCTS directly interacts with Rab8 and TNPO1 *via* pull-down assays using recombinant proteins. We made a recombinant chimera—His-13bCTS-GFP, which has His-tag, 13bCTS, and GFP from its N to C-terminus (Figs. 4*B*

and S1*C*). Recombinant chimeras—His-MBP-GFP and His-GFP—were used as negative controls (Fig. 4*B*). When bead-immobilized GST-TNPO1 was incubated with His-13bCTS-GFP or His-MBP-GFP, we found that TNPO1 alone retained a significant amount of 13bCTS (Fig. 4*E*), indicating a direct interaction. Furthermore, when bead-immobilized GST-TNPO1 was incubated with His-13bCTS-GFP or His-GFP together with His-Rab8-TN or His-Rab8-QL, we found that GST-TNPO1 pulled down much more His-13bCTS-GFP in the presence of His-Rab8-TN than His-Rab8-QL (Lane one and two of Fig. 4*F*). Furthermore, bead-immobilized GST-TNPO1 retained a significant amount of His-Rab8-TN only in the presence of His-13bCTS-GFP but not His-GFP (Lane two and four of Fig. 4*F*); under the same condition, GST-TNPO1 did not directly pull down a significant amount of His-Rab8-TN (Lane six of Fig. 4*F*), suggesting that TNPO1 might indirectly associate Rab8-TN *via* 13bCTS. Hence, our data suggest that Rab8-TN and TNPO1 could simultaneously and synergistically interact with 13bCTS directly; the three proteins might assemble into a ternary complex in which 13bCTS connects Rab8 and TNPO1.

### *Rab8 and TNPO1 are in the proximity of mitochondrion-localized 13bCTS*

To study the interaction of 13bCTS with Rab8 and TNPO1 in the cellular environment, we employed the proximity biotinylation assay using mitochondrion-located and TurboID-fused 13bCTS (46). TurboID-mediated biotinylation enables the detection of transient and weak protein interactions, and the relocalization of a bait protein (*e.g.*, 13bCTS) to the mitochondrial outer membrane can significantly reduce the background biotinylation due to the colocalization at its native compartment (*e.g.*, cilium) (47). To that end, first, we made the expression construct, Mito-CTS-TurboID-GFP, consisting of the mitochondrial outer membrane targeting sequence of Tom20 at the N-terminus (48), followed by a CTS fragment and the C-terminal TurboID-GFP tag (Fig. 5*A*). The CTS fragment was one of the following—13bCTS, 13bCTS-RVEP-4A, the CTS of fibrocystin (fCTS) (19), and fCTS-KTRK-4A (19). Among them, fCTS served as a positive control since it binds to Rab8 and TNPO1, while fCTS-KTRK-4A was a negative control since the KTRK-4A mutation abolished the ciliary localization of fCTS (19). Next, we demonstrated that these chimeras correctly localized to mitochondria when transiently expressed in RPE1 cells (Fig. 5*B*). Then, we individually transfected these constructs to HEK293T cells. After adding biotin, TurboID-biotinylated proteins were captured by streptavidin magnetic beads. Finally, bead-retained proteins were analyzed by immunoblotting (Fig. 5*C*). We found that Rab8 and TNPO1 were specifically biotinylated when 13bCTS or fCTS construct was used in transfection, supporting the interaction of Rab8-TN and TNPO1 with 13bCTS and fCTS on the mitochondrial

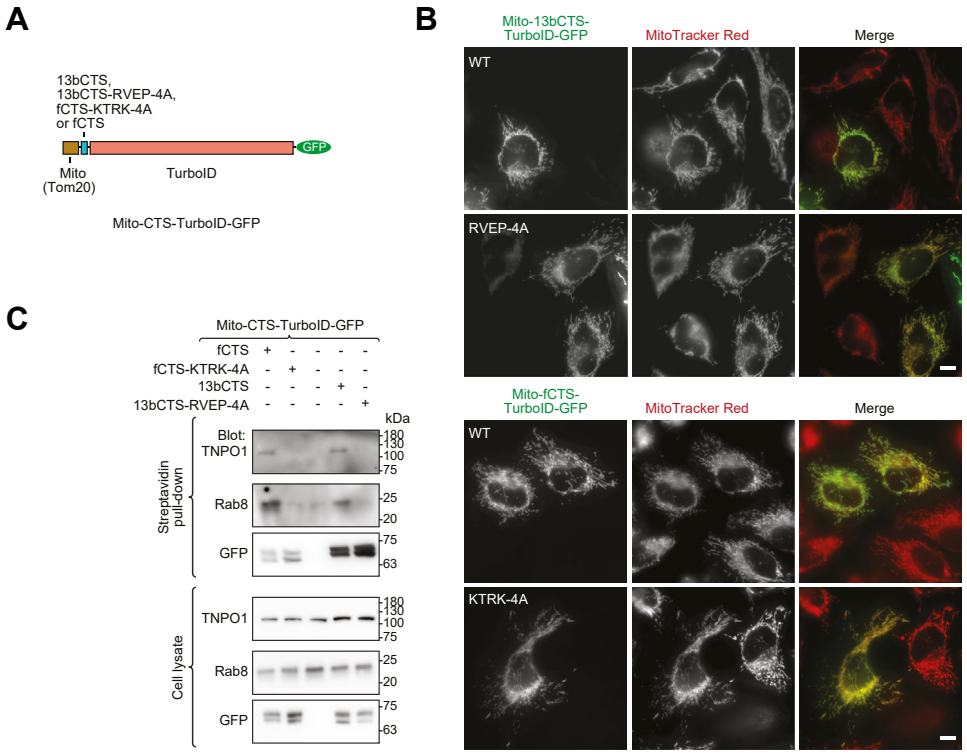


**Figure 5. Rab8 and TNPO1 are in the proximity of mitochondrion-localized 13bCTS.** *A*, a schematic diagram showing the domain organization of Mito-CTS-TurboID-GFP. The CTS can be that of Arl13b (13bCTS) or fibrocystin (fCTS) in WT or mutant form. *B*, Mito-CTS-TurboID-GFP correctly localizes to the mitochondrion. RPE1 cells were transiently transfected with Mito-13bCTS-TurboID-GFP, Mito-fCTS-TurboID-GFP, or their corresponding mutants. Cells were subsequently stained with MitoTracker Red (a mitochondrion marker) and imaged live. Scale bar, 10 μm. *C*, Mitochondrion-anchored 13bCTS and fCTS but not their mutants recruit endogenous Rab8 and TNPO1 to their proximity. Cells transiently expressing indicated Mito-CTS-TurboID-GFP were incubated with 50 μM biotin for 24 h. TurboID biotinylated proteins were subsequently pulled down by streptavidin magnetic beads, and bead-retained proteins were analyzed by immunoblotting. Molecular weight markers are labeled to the *right* of all immunoblots.

outer membrane. In contrast, in cells expressing the corresponding CTS mutant, 13bCTS-RVEP-4A or fCTS-KTRK-4A, we did not detect the biotinylation of Rab8 and TNPO1. Therefore, these results further support 13bCTS' interaction with Rab8-GDP and TNPO1, implying the formation of the ternary complex in the cellular environment.

### *The ciliary targeting of endogenous Arl13b requires Rab8 and TNPO1*

To evaluate the role of Rab8 and TNPO1 in the ciliary localization of Arl13b, we employed the lentivirus-transduced shRNA to knock down endogenous Rab8 and TNPO1. Compared to the control shRNA, Rab8 and TNPO1 shRNAs substantially reduced the endogenous level of target proteins in Western blot (Fig. 6, *A* and *B*). Importantly, the knockdown of Rab8 and TNPO1 did not affect the cellular level of endogenous Arl13b (Fig. 6*C*). We then co-stained the knockdown cells for the endogenous Arl13b and acetylated tubulin, a marker for the cilium (Fig. 6*D*). Quantification of Arl13b intensity at the cilium revealed that knockdown of Rab8 or TNPO1 significantly decreased the ciliary pool of endogenous Arl13b. Therefore, our knockdown data demonstrate that Rab8 and TNPO1 are essential for the ciliary targeting of Arl13b, supporting our hypothesis that they could function as the ciliary transport adaptor for Arl13b.

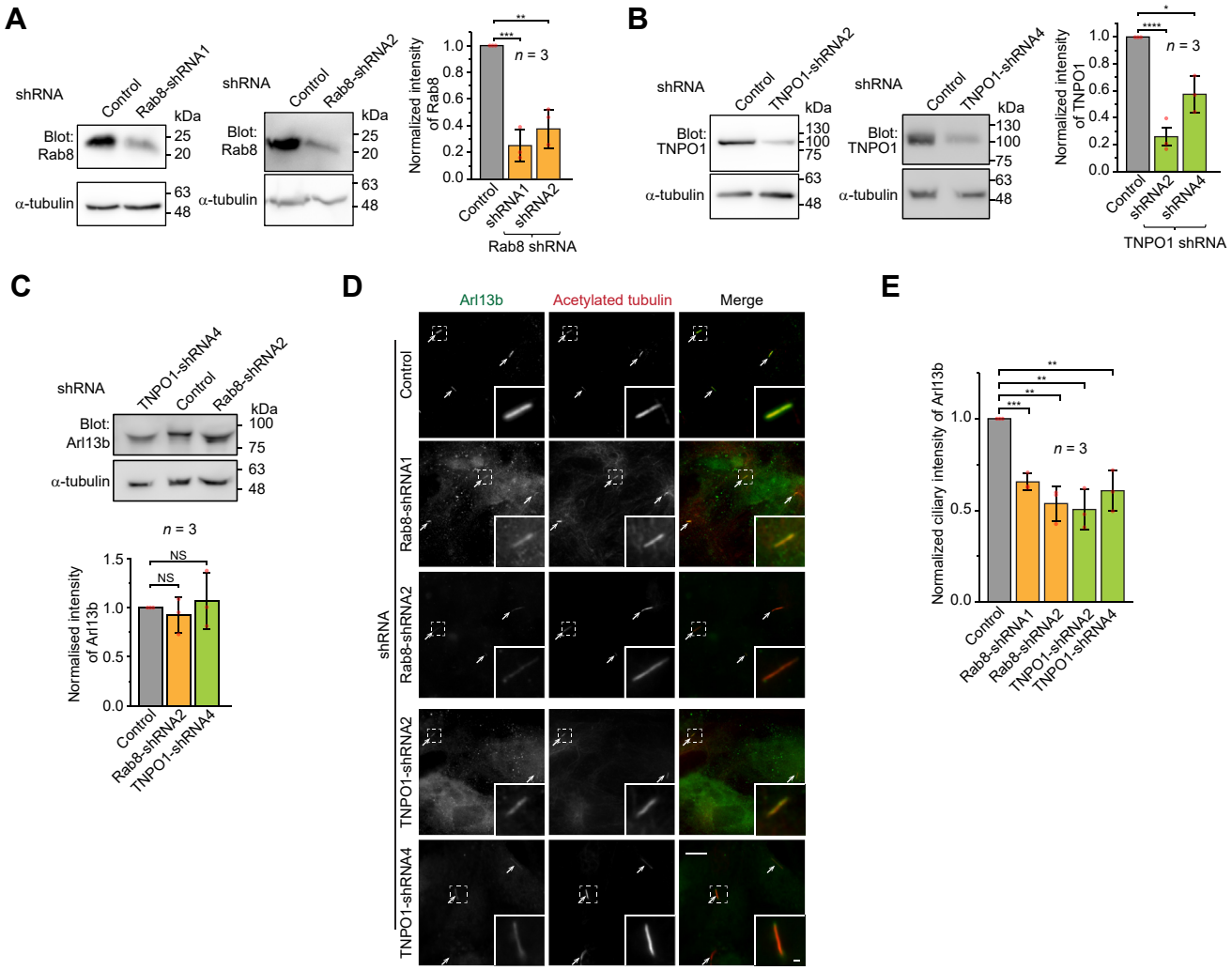


**Figure 6. Depletion of cellular Rab8 or TNPO1 decreases the ciliary localization of Arl13b.** All cells were RPE1 cells. *A* and *B*, the knockdown of endogenous Rab8 or TNPO1 by shRNAs. After lentivirus-mediated transduction of Rab8, TNPO1, or control shRNAs, cell lysates were subjected to immunoblotting for endogenous Rab8, TNPO1, or α-tubulin (loading control). The bar graph on the *right* shows the α-tubulin-normalized band intensities of Rab8 and TNPO1. $n = 3$ independent experiments. *C*, the knockdown of Rab8 or TNPO1 does not affect the cellular level of Arl13b. After lentivirus-mediated transduction of Rab8, TNPO1, or control shRNAs, cell lysates were subjected to immunoblotting for endogenous Arl13b or α-tubulin (loading control). The bar graph below shows the α-tubulin-normalized band intensities of Arl13b. $n = 3$ independent experiments. *D* and *E*, the knockdown of Rab8 or TNPO1 decreases the ciliary localization of Arl13b. After lentivirus-mediated transduction of Rab8, TNPO1, or control shRNAs, cells were immunostained for Arl13b and acetylated tubulin (*D*). *Arrows* indicate cilia. Scale bar, 10 μm. The boxed cilium is enlarged at the *lower right corner*. Scale bar, 1 μm. In (*E*), the fluorescence intensity of Arl13b at the cilium, marked by acetylated tubulin, was quantified and normalized by that in control shRNA-treated cells. Results are from $n = 3$ independent experiments with >30 cilia quantified. The ciliary intensity of Arl13b was normalized by the mean of the control panel. Molecular weight markers are labeled to the *right* of all immunoblots. In (*A*–*C*, *E*), the error bar represents the *mean* ± *SD*. *p*-values are from unpaired, two-tailed *t*-tests; NS, not significant; *$p \le 0.05$; **$p \le 0.005$; ***$p \le 0.0005$; ****$p \le 0.00005$.

## Discussion

The ciliary localization of Arl13b requires its C-terminal RVEP motif (23, 35–38). However, its cognate ciliary transport adaptor has been elusive. Here, we revealed that the RVEP motif constitutes an essential element of the CTS of Arl13b (13bCTS), consisting of a C-terminal stretch of 17 AAs. We found that 13bCTS is both necessary and sufficient for the ciliary localization of Arl13b. Further mutation and truncation of 13bCTS substantially reduce its ciliary localization. We discovered that Rab8 and TNPO1 bind to 13bCTS *via* the RVEP motif. Furthermore, we found that Rab8-GDP and TNPO1 can directly interact with 13bCTS simultaneously and synergistically (Fig. 4, *C–F*), suggesting that similar to other ciliary clients (19), Rab8-GDP, TNPO1, and 13bCTS might assemble into a ternary complex (Fig. 7*A*). Our current working model is that Rab8-GDP and TNPO1 simultaneously interact with not only 13bCTS but also each other. We have not detected a significant interaction between Rab8-GDP and TNPO1 in the absence of 13CTS (Fig. 4, *D* and *F*), consistent with our previous studies (19). However, we propose that engaging 13bCTS possibly changes the conformation Rab8-GDP and TNPO1, resulting in their interaction. Hence, the synergistic effect might be attributed to the 13bCTS-induced interaction between TNPO1 and Rab8-GDP, which should significantly enhance the stability of the ternary complex. However, confirming our molecular model of the ternary complex requires future work.

We also demonstrated that the ciliary localization of Arl13b requires both Rab8 and TNPO1. Together, our data suggest that Rab8 and TNPO1 might function as the ciliary transport adaptor of Arl13b. Therefore, in addition to fibrocystin, prRDH, rhodopsin, and RP2 (19), our current discovery further expands the list of ciliary clients of Rab8 and TNPO1. So, we expect more ciliary clients of Rab8 and TNPO1 to be uncovered. Our previous model can explain how Rab8-GDP and TNPO1 transport Arl13b to the cilium (6, 19) (Fig. 7*B*). First, palmitoylated Arl13b associates and diffuses along the PM. Then, at the periciliary membrane, the PM-associated Arl13b simultaneously interacts with TNPO1 and Rab8-GDP to assemble the ternary complex. Next, TNPO1 facilitates the translocation of the ternary complex through the membrane diffusion barrier imposed by the transition zone at the ciliary base. After the import translocation, a cilium-localized Rab8 guanine nucleotide exchange factor (Rab8-GEF), such as Rabin8 (49) or RPGR (50), changes the guanine nucleotide of Rab8 from GDP to GTP. Consequently, the ternary complex disassembles, and Arl13b is released to the ciliary membrane since Rab8-GTP no longer interacts with 13bCTS (Fig. 4, *A*, *C*, *D* and *F*). Finally, with the export translocation of TNPO1, the ciliary exit of Arl13b is blocked by the ciliary membrane diffusion barrier (transition zone), resulting in a dynamic and freely diffusible pool of Arl13b on the ciliary membrane. Similarly, Rab8-GTP also accumulates within the cilium. Our model shares similarities with the nucleocytoplasmic trafficking pathway, in which Ran-GTP disassembles the importin-cargo complex in the nucleus after crossing the nuclear pores (51).

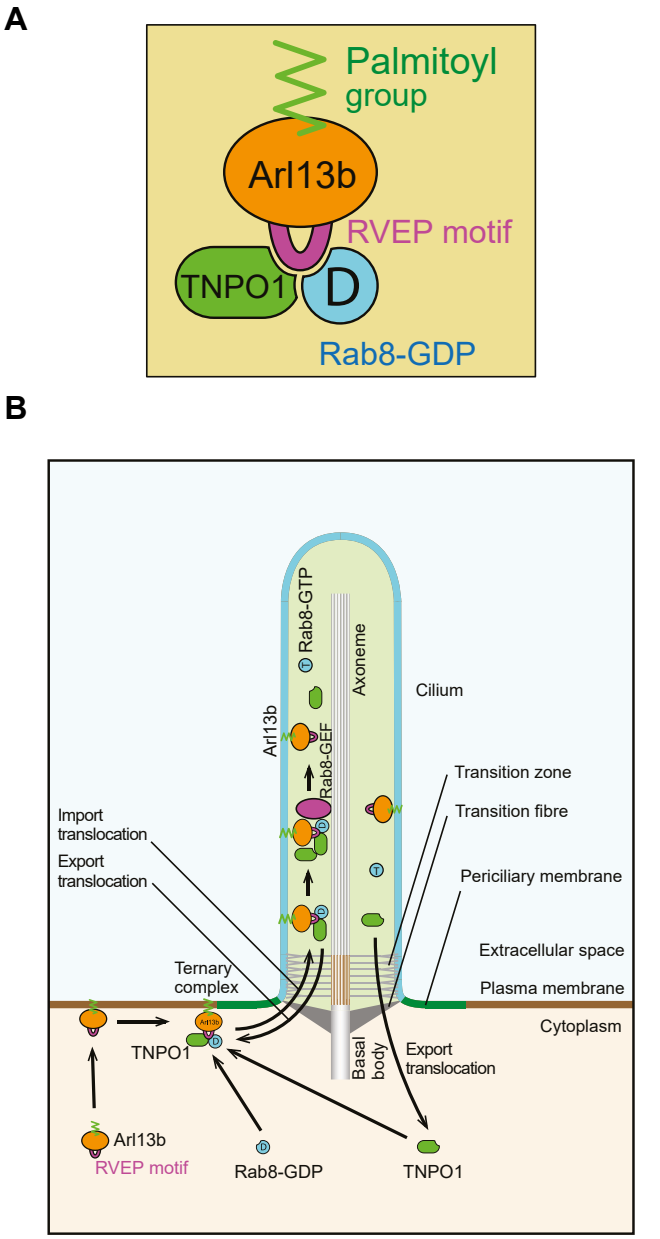


**Figure 7. Our working model on the molecular organization and trafficking mechanism of the ternary complex.** *A*, the Rab8-GDP, TNPO1, and 13bCTS ternary complex. Rab8-GDP and TNPO1 simultaneously interact with 13bCTS within the C-terminal loop of Arl13b. Such interactions probably induce the conformation changes of Rab8-GDP and TNPO1, so they also interact with each other. *B*, Rab8 and TNPO1 function as ciliary transport adaptors and target Arl13b to the cilium. Refer to the text in the Discussion for details.

Previous studies proposed Tulp3 as the ciliary transport adaptor of Arl13b (31–33), although their direct interaction has not been confirmed. Recently, Palicharla *et al.* (34) reported that the N-terminal amphipathic helix, AA1-21, interacts with Tulp3 and functions as a potential CTS of Arl13b. They further showed that deleting the two N-terminal amphipathic helical regions within AA1-21 abolished the ciliary localization of Arl13b. However, the authors did not rule out the possibility that the deletion could affect the

palmitoylation, which is essential for the ciliary localization of Arl13b (C8S/C9S in Fig. 1*A*) (43). Notably, the authors did not demonstrate the sufficiency of AA1-21 in ciliary targeting by testing if it can target a non-ciliary reporter to the cilium. Our data suggest that AA1-21 might be neither necessary nor sufficient for the ciliary localization of Arl13b. The negative ciliary localization of AA1-245 and the full-length with RVEP-4A mutation, both with an intact N-terminus including AA1-21, demonstrates that AA1-21 is insufficient for ciliary targeting (Fig. 1, *A* and *C*). On the other hand, the robust ciliary localization of CD8a-13bCTS (Fig. 3, *A* and *B*) demonstrates that AA1-21 is unnecessary for ciliary targeting other than palmitoylation and membrane attachment. Therefore, we think AA1-21 or the N-terminal amphipathic helix might not function as the CTS, and 13bCTS might be the sole CTS of Arl13b. Further investigation is required to define the Tulp3-binding region in Arl13b. Since Arl13b has two potential transport adaptors, Tupl3 and Rab8-TNPO1, whether they function sequentially or simultaneously would be an interesting question for the future work.

## Experimental procedures

### DNA plasmids

Please see Table S1 for all the plasmids used in this study.

### Antibodies

Mouse mAbs against acetylated tubulin (Merck, #T6793, 1:1000 for immunofluorescence or IF), α-tubulin (Developmental Studies Hybridoma Bank, clone 12G10, 1:1000 for Western blot or WB), GFP (Santa Cruz, #sc9996, 1:1000 for WB), pericentrin (Abcam, #ab4448, 1:1000 for IF), TNPO1 (Abcam, #ab10303, 1:3000 for WB), Rab8 (BD biosciences, #610844, 1:1000 for WB), and CD8a (Developmental Studies Hybridoma Bank, clone OKT8, 1:200 for IF). Rabbit polyclonal antibodies against Arl13b (19) (1:1000 for IF and WB and Proteintech, 17711-1-AP, 1:1000 for WB) and GFP (52). HRP-conjugated goat anti-mouse and anti-rabbit IgG antibodies were purchased from Bio-Rad. HRP-conjugated protein A was purchased from Abcam. Alexa Fluor-conjugated goat anti-mouse and anti-rabbit IgG antibodies (1:500 for IF) were purchased from Invitrogen.

### Cell culture and transfection

RPE1 (hTERT-RPE1) and HEK293T cells were from American Type Culture Collection. HEK293FT cells were from Thermo Fisher Scientific. RPE1 cells were cultured in Dulbecco's Modified Eagle's Medium (DMEM) and Ham's F12 mixture medium supplemented with 10% fetal bovine serum (FBS). HEK293T cells were cultured in DMEM supplemented with 10% FBS. HEK293FT were cultured in DMEM supplemented with 10% FBS and 50 μg/ml G418 (Thermo Fisher Scientific). Transfection of plasmid DNA was performed using polyethylenimine (Polysciences) or Lipofectamine 2000 (Thermo Fisher Scientific) according to the manufacturer's protocol. Ciliogenesis was induced by incubating cells under serum starvation (without FBS) for 48 h. For the live cell imaging under the TIRF or wide-field microscope, cells were grown on Φ 35 mm glass-bottom Petri dish in the $CO_2$ independent medium (Thermo Fisher Scientific) supplemented with 10% FBS and 4 mM glutamine.

### Lentivirus-transduced knockdown of TNPO1 and Rab8

Endogenous TNPO1 and Rab8 were depleted by lentivirus-mediated transduction of shRNA. Control shRNA, TNPO1 shRNA #2 and #4, and Rab8 shRNA#1 and #2 in pLKO.1 vector and packaging plasmids pLP1, pLP2, and pLP/VSVG (Thermo Fisher Scientific) were transiently transfected to HEK293FT cells using polyethylenimine. Lentiviruses were harvested 36 and 60 h post-transfection, filtered using 0.45-μm filter (Sartorius), and immediately used to infect RPE1 cells. RPE1 cells seeded in a six-well plate were infected twice every 24 h with filtered lentiviruses using 8 μg/ml hexadimethrine bromide (Sigma-Aldrich #H9268). The cells were then split into a 24-well plate for Western blot analysis of knockdown efficiency or onto coverslips followed by serum starvation for 48 h to induce ciliogenesis before immunolabeling.

### Purification of His- and GST-tagged fusion proteins

pET30ax DNA plasmids encoding His-GFP, His-13bCTS-GFP, His-AA1-245-GFP, His-AA193-428-GFP, His-Rab-TN, and His-Rab-QL were transformed into BL21 *E. coli* cells. Transformed bacteria were induced by isopropyl β-D-1-Thiogalactopyranoside, subsequently pelleted, and lysed by sonication in the lysis buffer (50 mM Tris, pH 8.0, 100 mM NaCl). Next, the lysate was cleared by centrifugation, and the supernatant was incubated with pre-washed Ni-NTA agarose beads (QIAGEN) in the presence of 10 mM imidazole in a cold room overnight. After beads were washed with the lysis buffer containing 25 mM imidazole, the bound protein was eluted with the lysis buffer containing 250 mM imidazole. The eluted protein was dialyzed and concentrated by ultrafiltration spin column (GE Healthcare), quantified by Coomassie gel staining, and stored at −20 °C until use.

pGEB and pGEX-4T1 DNA plasmids encoding GST-TNPO1, GST-Rab-TN, and GST-Rab-QL were transformed into BL21 *E. coli* cells, induced by isopropyl β-D-1-Thiogalactopyranoside, subsequently pelleted and lysed by sonication in the lysis buffer (50 mM Tris, pH 8.0, 100 mM NaCl). Next, the lysate was cleared by centrifugation, and the supernatant was incubated with pre-washed glutathione Sepharose (GE Healthcare) in a cold room overnight. After beads were washed by the lysis buffer, the bound protein was quantified by Coomassie gel staining and stored at −20 °C until use.

### GST pull-down assay

HEK293T cells were used to express various tagged proteins. After 24 to 36 h of transfection, as mentioned above, cells were lysed in the lysis buffer containing 40 mM HEPES pH 7.3100 mM NaCl and 1% Triton X-100 1 mM DTT. The resulting lysates were incubated in a cold room for 30 min, centrifuged at 17,000*g* for 30 min, and the supernatants were

incubated with 10 to 40 μg of GST fusion protein on glutathione Sepharose beads overnight. The beads were washed with lysis buffer, and the bound proteins were eluted by boiling in the SDS sample buffer and resolved in SDS-PAGE. The separated proteins were transferred to a polyvinyl difluoride membrane (Bio-Rad) and subsequently incubated with primary and HRP-conjugated secondary antibodies. Images of Western blots and corresponding molecular weight markers were acquired under chemiluminescence and white light imaging mode, respectively, using a cooled charge-coupled device of LAS-4000 (GE Healthcare Life Sciences).

### *TurboID proximity biotinylation assay*

HEK293T cells were used to express various Mito-CTS-TurboID-GFP proteins. After 24 h of transfection, cells were incubated with 50 μM biotin for 24 h. Next, cells were pelleted, washed 3 × with ice-cold PBS, and resuspended in the lysis buffer (20 mM Tris pH 7.3, 100 mM NaCl, 1% Triton X-100, 1% NP40, 0.1% SDS, 1 mM DTT). The cell and lysis buffer mixture was subsequently incubated in the cold room for 30 min followed by centrifugation. The supernatant was incubated with prewashed streptavidin magnetic beads (Thermo Fisher Scientific) in the cold room overnight. The magnetic beads were washed 3 × with the lysis buffer, 3 × with the lysis buffer containing 500 mM NaCl, and 3 × with the lysis buffer containing 4 mM Urea. The bound proteins were eluted by boiling in the SDS sample buffer containing 3 mM biotin, resolved by the SDS-PAGE, and subjected to Western blot analysis as mentioned previously.

### *Wide-field fluorescence microscopy*

RPE1 cells were seeded on No. 1.5 Φ 12 or 25-mm coverslips in a 24- or six-well plate, respectively. Cells were serum-starved for 48 h to induce ciliogenesis, fixed with 4% paraformaldehyde in PBS, and subsequently neutralized with ammonium chloride. The cells were incubated with primary antibodies diluted in the antibody dilution buffer, consisting of PBS supplemented with 5% FBS and 2% bovine serum albumin and 0.1% Saponin (Sigma-Aldrich). After washing, cells were incubated with secondary antibodies diluted in the antibody dilution buffer. The coverslips were mounted in Mowiol 4 to 88 (EMD Millipore) after extensive washes using PBS. For surface labeling, cells grown on coverslips were incubated on ice with CD8a monoclonal antibody, washed with ice-cold PBS, fixed, and subjected to immunofluorescence labeling as described previously. Cells were imaged under an inverted wide-field Olympus IX83 microscope system equipped with a Plan Apo oil objective lens (63× or 100×, NA 1.40), a motorized stage, a focus drift correction device, motorized filter cubes, a scientific complementary metal oxide semiconductor camera (Neo; Andor Technology), and a 200-W metal halide excitation light source (Lumen Pro 200; Prior Scientific). Dichroic mirrors and filters in filter turrets were optimized for GFP and Alexa Fluor 488, mCherry and Alexa Fluor 594, and Alexa Fluor 647. The microscope system was controlled by MetaMorph software (Molecular Devices).

To image MitoTracker Red and stained Mito-CTS-TurboID-GFP expressing cells, RPE1 cells were grown on Φ 35 mm glass-bottom Petri-dish and transfected with Mito-CTS-TurboID-GFP constructs. Cells were treated with 25 nM MitoTracker Red (Thermo Fisher Scientific) for 20 min at 37 °C. After several washes with PBS, live-cell imaging was performed under the wide-field microscope.

### *TIRF microscopy*

RPE1 cells were grown on Φ 35 mm glass-bottom Petri-dish and transfected with PAL-GFP WT or C8S/C9S constructs. Live cell imaging was acquired under the wide-field or TIRF mode using a TIRF microscope comprising Zeiss Observer Z1 inverted microscope equipped with a 100×/NA 1.46 objective lens (plan apochromat), a fully motorized stage, Zeiss Laser TIRF three module, 30 mW solid-state laser (488 nm), Zeiss Filter Set 52 HE (excitation filter: BP 488/20, dichroic mirror: FT505, and emission filter 530/550), and an electron-multiplying charge-coupled device (Evolve 512). The microscope system was controlled under Zen software (Zeiss).

### *Quantification of the* CPIR

The calculation of the *CPIR* was performed as described previously (19). Briefly, the line intensity profile of the cilium was determined by drawing a ∼1 μm thick line orthogonally across the cilium, and the maximum value ($I_{max}$) was obtained. The mean intensity of PM ($I_{PM}$) and the background value ($I_{background}$) were similarly acquired by drawing a circular ROI on the PM and background region, respectively. The *CPIR* of the membrane protein is defined as $(I_{max} - I_{PM})/(I_{PM} - I_{background})$ and indicates its relative enrichment along the unit length of cilium normalized to its PM expression level.

### *Image and statistical analysis*

All image analysis was conducted using ImageJ (https://imagej.nih.gov/ij/). Data analysis and graphs were plotted using OriginPro 9 (OriginLab). Images were randomly acquired. The sample size $n$ is indicated wherever applicable in figures or corresponding legends. Data are presented as the *mean* ± *SD*. The two-tailed unpaired *t*-tests were conducted in Excel (Microsoft). A $p$ value ≤ 0.05 was considered statistically significant.

## Data availability

All data are included in the manuscript.

*Supporting information*—This article contains supporting information.

*Acknowledgments*—We want to thank the following researchers for sharing their DNA plasmids with us: A. Ting (Stanford University, USA), D. Root (Broad Institute, USA), and S. Royle (University of Warwick, UK).

*Author contributions*—L. L., D. M., and V. M. conceptualization; D. M., V. M., and L. L. methodology; D. M. and V. M. formal

analysis, investigation, and validation; D. M. and L. L. visualization; L. L. and D. M. writing; L. L. supervision, project administration, and funding acquisition.

*Funding and additional information*—This research is supported by the Ministry of Education, Singapore, under its MOE Tier 2 MOE-T2EP30221-0001 and Tier 1 RG25/22.

*Conflict of interest*—The authors declare that they have no conflicts of interest with the contents of this article.

*Abbreviations*—The abbreviations used are: CC, coiled-coil region; CPIR, cilium to the PM intensity ratio; CTS, ciliary targeting sequence; DMEM, Dulbecco's Modified Eagle's Medium; FBS, fetal bovine serum; IDR, intrinsically disordered region; PM, plasma membrane; PRR, proline-rich region; prRDH, photoreceptor retinol dehydrogenase.

## References


1. Nachury, M. V., and Mick, D. U. (2019) Establishing and regulating the composition of cilia for signal transduction. *Nat. Rev. Mol. Cell Biol.* **20**, 389–405
2. Anvarian, Z., Mykytyn, K., Mukhopadhyay, S., Pedersen, L. B., and Christensen, S. T. (2019) Cellular signalling by primary cilia in development, organ function and disease. *Nat. Rev. Nephrol.* **15**, 199–219
3. Reiter, J. F., and Leroux, M. R. (2017) Genes and molecular pathways underpinning ciliopathies. *Nat. Rev. Mol. Cell Biol.* **18**, 533–547
4. Madhivanan, K., and Aguilar, R. C. (2014) Ciliopathies: the trafficking connection. *Traffic* **15**, 1031–1056
5. Hildebrandt, F., Benzing, T., and Katsanis, N. (2011) Ciliopathies. *N. Engl. J. Med.* **364**, 1533–1543
6. Lu, L., and Madugula, V. (2018) Mechanisms of ciliary targeting: entering importins and Rabs. *Cell. Mol. Life Sci.* **75**, 597–606
7. Nachury, M. V., Seeley, E. S., and Jin, H. (2010) Trafficking to the ciliary membrane: how to get across the periciliary diffusion barrier? *Annu. Rev. Cell Dev. Biol.* **26**, 59–87
8. Hsiao, Y. C., Tuz, K., and Ferland, R. J. (2012) Trafficking in and to the primary cilium. *Cilia* **1**, 4
9. Long, H., and Huang, K. (2019) Transport of ciliary membrane proteins. *Front Cell Dev. Biol.* **7**, 381
10. Badgandi, H. B., Hwang, S. H., Shimada, I. S., Loriot, E., and Mukhopadhyay, S. (2017) Tubby family proteins are adapters for ciliary trafficking of integral membrane proteins. *J. Cell Biol.* **216**, 743–760
11. Mukhopadhyay, S., Wen, X., Ratti, N., Loktev, A., Rangell, L., Scales, S. J., *et al.* (2013) The ciliary G-protein-coupled receptor Gpr161 negatively regulates the sonic hedgehog pathway via cAMP signaling. *Cell* **152**, 210–223
12. Mukhopadhyay, S., Wen, X., Chih, B., Nelson, C. D., Lane, W. S., Scales, S. J., *et al.* (2010) TULP3 bridges the IFT-A complex and membrane phosphoinositides to promote trafficking of G protein-coupled receptors into primary cilia. *Genes Dev.* **24**, 2180–2193
13. Barbeito, P., Tachibana, Y., Martin-Morales, R., Moreno, P., Mykytyn, K., Kobayashi, T., *et al.* (2021) HTR6 and SSTR3 ciliary targeting relies on both IC3 loops and C-terminal tails. *Life Sci. Alliance* **4**, e202000746
14. Hilgendorf, K. I., Johnson, C. T., Mezger, A., Rice, S. L., Norris, A. M., Demeter, J., *et al.* (2019) Omega-3 fatty acids activate ciliary FFAR4 to control adipogenesis. *Cell* **179**, 1289–1305.e21
15. Wu, C. T., Hilgendorf, K. I., Bevacqua, R. J., Hang, Y., Demeter, J., Kim, S. K., *et al.* (2021) Discovery of ciliary G protein-coupled receptors regulating pancreatic islet insulin and glucagon secretion. *Genes Dev.* **35**, 1243–1255
16. Fan, S., Fogg, V., Wang, Q., Chen, X. W., Liu, C. J., and Margolis, B. (2007) A novel Crumbs3 isoform regulates cell division and ciliogenesis via importin beta interactions. *J. Cell Biol.* **178**, 387–398
17. Dishinger, J. F., Kee, H. L., Jenkins, P. M., Fan, S., Hurd, T. W., Hammond, J. W., *et al.* (2010) Ciliary entry of the kinesin-2 motor KIF17 is regulated by importin-beta2 and RanGTP. *Nat. Cell Biol.* **12**, 703–710
18. Follit, J. A., Li, L., Vucica, Y., and Pazour, G. J. (2010) The cytoplasmic tail of fibrocystin contains a ciliary targeting sequence. *J. Cell Biol.* **188**, 21–28
19. Madugula, V., and Lu, L. (2016) A ternary complex comprising transportin1, Rab8 and the ciliary targeting signal directs proteins to ciliary membranes. *J. Cell Sci.* **129**, 3922–3934
20. Caspary, T., Larkins, C. E., and Anderson, K. V. (2007) The graded response to sonic hedgehog depends on cilia architecture. *Dev. Cell* **12**, 767–778
21. Cantagrel, V., Silhavy, J. L., Bielas, S. L., Swistun, D., Marsh, S. E., Bertrand, J. Y., *et al.* (2008) Mutations in the cilia gene ARL13B lead to the classical form of Joubert syndrome. *Am. J. Hum. Genet.* **83**, 170–179
22. Larkins, C. E., Aviles, G. D., East, M. P., Kahn, R. A., and Caspary, T. (2011) Arl13b regulates ciliogenesis and the dynamic localization of Shh signaling proteins. *Mol. Biol. Cell* **22**, 4694–4703
23. Nozaki, S., Katoh, Y., Terada, M., Michisaka, S., Funabashi, T., Takahashi, S., *et al.* (2017) Regulation of ciliary retrograde protein trafficking by the Joubert syndrome proteins ARL13B and INPP5E. *J. Cell Sci.* **130**, 563–576
24. Humbert, M. C., Weihbrecht, K., Searby, C. C., Li, Y., Pope, R. M., Sheffield, V. C., *et al.* (2012) ARL13B, PDE6D, and CEP164 form a functional network for INPP5E ciliary targeting. *Proc. Natl. Acad. Sci. U. S. A.* **109**, 19691–19696
25. Chavez, M., Ena, S., Van Sande, J., de Kerchove d'Exaerde, A., Schurmans, S., and Schiffmann, S. N. (2015) Modulation of ciliary phosphoinositide content regulates trafficking and sonic hedgehog signaling output. *Dev. Cell* **34**, 338–350
26. Garcia-Gonzalo, F. R., Phua, S. C., Roberson, E. C., Garcia, G., 3rd, Abedin, M., Schurmans, S., *et al.* (2015) Phosphoinositides regulate ciliary protein trafficking to modulate hedgehog signaling. *Dev. Cell* **34**, 400–409
27. Gotthardt, K., Lokaj, M., Koerner, C., Falk, N., Giessl, A., and Wittinghofer, A. (2015) A G-protein activation cascade from Arl13B to Arl3 and implications for ciliary targeting of lipidated proteins. *Elife* **4**, e11859
28. Ismail, S. A., Chen, Y. X., Miertzschke, M., Vetter, I. R., Koerner, C., and Wittinghofer, A. (2012) Structural basis for Arl3-specific release of myristoylated ciliary cargo from UNC119. *EMBO J.* **31**, 4085–4094
29. Ismail, S. A., Chen, Y. X., Rusinova, A., Chandra, A., Bierbaum, M., Gremer, L., *et al.* (2011) Arl2-GTP and Arl3-GTP regulate a GDI-like transport system for farnesylated cargo. *Nat. Chem. Biol.* **7**, 942–949
30. Wright, K. J., Baye, L. M., Olivier-Mason, A., Mukhopadhyay, S., Sang, L., Kwong, M., *et al.* (2011) An ARL3-UNC119-RP2 GTPase cycle targets myristoylated NPHP3 to the primary cilium. *Genes Dev.* **25**, 2347–2360
31. Hwang, S. H., Somatilaka, B. N., Badgandi, H., Palicharla, V. R., Walker, R., Shelton, J. M., *et al.* (2019) Tulp3 regulates renal cystogenesis by trafficking of cystoproteins to cilia. *Curr. Biol.* **29**, 790–802.e5
32. Legue, E., and Liem, K. F., Jr. (2019) Tulp3 is a ciliary trafficking gene that regulates polycystic kidney disease. *Curr. Biol.* **29**, 803–812.e5
33. Han, S., Miyoshi, K., Shikada, S., Amano, G., Wang, Y., Yoshimura, T., *et al.* (2019) TULP3 is required for localization of membrane-associated proteins ARL13B and INPP5E to primary cilia. *Biochem. Biophys. Res. Commun.* **509**, 227–234
34. [preprint] Palicharla, V. R., Hwang, S.-H., Somatilaka, B. N., Badgandi, H. B., Legué, E., Tran, V. M., *et al.* (2021) Interactions between TULP3 tubby domain cargo site and ARL13B amphipathic helix promote lipidated protein transport to cilia. *bioRxiv*. https://doi.org/10.1101/2021.05.25.445488
35. Cevik, S., Sanders, A. A., Van Wijk, E., Boldt, K., Clarke, L., van Reeuwijk, J., *et al.* (2013) Active transport and diffusion barriers restrict Joubert syndrome-associated ARL13B/ARL-13 to an Inv-like ciliary membrane subdomain. *PLoS Genet.* **9**, e1003977
36. Higginbotham, H., Guo, J., Yokota, Y., Umberger, N. L., Su, C. Y., Li, J., *et al.* (2013) Arl13b-regulated cilia activities are essential for polarized radial glial scaffold formation. *Nat. Neurosci.* **16**, 1000–1007
37. Mariani, L. E., Bijlsma, M. F., Ivanova, A. A., Suciu, S. K., Kahn, R. A., and Caspary, T. (2016) Arl13b regulates Shh signaling from both inside and outside the cilium. *Mol Biol Cell* **27**, 3780–3790

38. Gigante, E. D., Taylor, M. R., Ivanova, A. A., Kahn, R. A., and Caspary, T. (2020) ARL13B regulates sonic hedgehog signaling from outside primary cilia. *Elife* **9**, e50434
39. Kahn, R. A., East, M. P., and Francis, J. W. (2014) ARF-like (ARL) proteins. In: Wittinghofer, A., ed. *Ras Superfamily Small G Proteins: Biology and Mechanisms 2: Transport*, Springer International Publishing, Cham: 215–251
40. Donaldson, J. G., and Jackson, C. L. (2011) ARF family G proteins and their regulators: roles in membrane transport, development and disease. *Nat. Rev. Mol. Cell Biol.* **12**, 362–375
41. Kahn, R. A., Cherfils, J., Elias, M., Lovering, R. C., Munro, S., and Schurmann, A. (2006) Nomenclature for the human Arf family of GTP-binding proteins: ARF, ARL, and SAR proteins. *J. Cell Biol.* **172**, 645–650
42. Sztul, E., Chen, P. W., Casanova, J. E., Cherfils, J., Dacks, J. B., Lambright, D. G., *et al.* (2019) ARF GTPases and their GEFs and GAPs: concepts and challenges. *Mol. Biol. Cell* **30**, 1249–1271
43. Cevik, S., Hori, Y., Kaplan, O. I., Kida, K., Toivenon, T., Foley-Fisher, C., *et al.* (2010) Joubert syndrome Arl13b functions at ciliary membranes and stabilizes protein transport in Caenorhabditis elegans. *J. Cell Biol.* **188**, 953–969
44. Roy, K., Jerman, S., Jozsef, L., McNamara, T., Onyekaba, G., Sun, Z., *et al.* (2017) Palmitoylation of the ciliary GTPase ARL13b is necessary for its stability and its role in cilia formation. *J. Biol. Chem.* **292**, 17703–17717
45. Peranen, J., Auvinen, P., Virta, H., Wepf, R., and Simons, K. (1996) Rab8 promotes polarized membrane transport through reorganization of actin and microtubules in fibroblasts. *J. Cell Biol.* **135**, 153–167
46. Branon, T. C., Bosch, J. A., Sanchez, A. D., Udeshi, N. D., Svinkina, T., Carr, S. A., *et al.* (2018) Efficient proximity labeling in living cells and organisms with TurboID. *Nat. Biotechnol.* **36**, 880–887
47. Gillingham, A. K., Bertram, J., Begum, F., and Munro, S. (2019) *In vivo* identification of GTPase interactors by mitochondrial relocalization and proximity biotinylation. *Elife* **8**, e45916
48. Kanaji, S., Iwahashi, J., Kida, Y., Sakaguchi, M., and Mihara, K. (2000) Characterization of the signal that directs Tom20 to the mitochondrial outer membrane. *J. Cell Biol.* **151**, 277–288
49. Hattula, K., Furuhjelm, J., Arffman, A., and Peranen, J. (2002) A Rab8-specific GDP/GTP exchange factor is involved in actin remodeling and polarized membrane transport. *Mol. Biol. Cell* **13**, 3268–3280
50. Murga-Zamalloa, C. A., Atkins, S. J., Peranen, J., Swaroop, A., and Khanna, H. (2010) Interaction of retinitis pigmentosa GTPase regulator (RPGR) with RAB8A GTPase: implications for cilia dysfunction and photoreceptor degeneration. *Hum. Mol. Genet.* **19**, 3591–3598
51. Stewart, M. (2007) Molecular mechanism of the nuclear protein import cycle. *Nat. Rev. Mol. Cell Biol.* **8**, 195–208
52. Mahajan, D., Tie, H. C., Chen, B., and Lu, L. (2019) Dopey1-Mon2 complex binds to dual-lipids and recruits kinesin-1 for membrane trafficking. *Nat. Commun.* **10**, 3218